Vascular and tissue changes of magnetic susceptibility in the mouse brain after transient cerebral ischemia

Vaas, Markus ; Deistung, Andreas ; Reichenbach, Jürgen R ; Keller, Annika ; Kipar, Anja ; Klohs, Jan

Abstract: Magnetic resonance imaging (MRI) is an important aid for physicians in the diagnosis and management of patients with acute ischemic stroke. Quantitative susceptibility mapping (QSM) has been recently introduced as a novel MRI post-processing technique of gradient recalled echo (GRE) data. QSM yields quantitative maps of the corresponding underlying magnetic susceptibility distribution. QSM is useful for depicting the anatomy and for detecting brain abnormalities. But its utility in the context of ischemic stroke has not been extensively characterized. We tested the ability of QSM to characterize tissue changes in the transient middle cerebral artery occlusion (tMCAO) model of cerebral ischemia. We acquired high resolution GRE of mice brains at different time points after tMCAO for computation of QSM and MR frequency maps, and compared these maps with DWI and multi-slice multi-echo imaging acquired with the same animals. Prominent vessels with increased magnetic susceptibility were visible on frequency and magnetic susceptibility maps surrounding the lesion at all times (mostly visible at >12h after reperfusion). Immunohistological examination revealed compressed capillaries and prominent vessels after reestablishing reperfusion may indicate a compensatory effect. In addition, on both contrast maps regions of decreased magnetic susceptibility delineated at 24h and 48h after reperfusion that were distinctly different from the lesions seen on maps of the apparent diffusion coefficient (ADC) and T2 relaxation time constant. Since QSM can be performed without additional acquisition time in the course of acute stroke MRI examination, it may provide complementary information for the diagnostic follow-up of cerebral ischemia.

DOI: https://doi.org/10.1007/s12975-017-0591-x

Originally published at:
Vaas, Markus; Deistung, Andreas; Reichenbach, Jürgen R; Keller, Annika; Kipar, Anja; Klohs, Jan (2018). Vascular and tissue changes of magnetic susceptibility in the mouse brain after transient cerebral ischemia. Translational Stroke Research, 9(4):426-435.
DOI: https://doi.org/10.1007/s12975-017-0591-x

Vascular and tissue changes of magnetic susceptibility in the mouse brain after transient cerebral ischemia

Markus Vaas[1,2], PhD; Andreas Deistung[3,4,5], PhD; Jürgen R. Reichenbach[3,5], PhD; Annika Keller[7], PhD; Anja Kipar[8], Dr. med. vet. habil; Jan Klohs[1,2], PhD

[1]Institute for Biomedical Engineering, ETH & University of Zurich, 8093 Zurich, Switzerland

[2]Neuroscience Center Zurich, University of Zurich and ETH Zurich, Switzerland

[3]Medical Physics Group, Institute of Diagnostic and Interventional Radiology, University Hospital Jena, 07743 Jena, Germany

[4]Section of Experimental Neurology, Department of Neurology, Essen University Hospital, 45147 Essen, Germany

[5]Erwin L. Hahn Institute for Magnetic Resonance Imaging, University Duisburg-Essen, 45141 Essen, Germany

[6]Michael Stifel Center for Data-driven and Simulation Science Jena, Friedrich Schiller University Jena, 07743 Jena, Germany

[7]Division of Neurosurgery. University Hospital Zurich, 8091 Zurich, Switzerland

[8]Institute of Veterinary Pathology, University of Zurich, 8057 Zurich, Switzerland

Correspondence to:

Jan Klohs, Institute for Biomedical Engineering, University of Zurich and ETH, Vladimir-Prelog-Weg 4, CH-8093 Zurich, Switzerland

Phone: +41 44 633 76 29, Fax: +41 44 633 11 87

E-mail: klohs@biomed.ee.ethz.ch

ORCID Jan Klohs: 0000-0003-4065-2807

Keywords: quantitative susceptibility mapping; MR frequency; magnetic resonance imaging; mice; middle cerebral artery occlusion; ischemia

Acknowledgements

This study was by the Swiss National Science Foundation (Grant PZ00P3_136822) and the Hartmann-Müller Foundation.

Abstract

Magnetic resonance imaging (MRI) is an important aid for physicians in the diagnosis and management of patients with acute ischemic stroke. Quantitative susceptibility mapping (QSM) has been recently introduced as a novel MRI post-processing technique of gradient recalled echo (GRE) data. QSM yields quantitative maps of the corresponding underlying magnetic susceptibility distribution. QSM is useful for depicting the anatomy and for detecting brain abnormalities. But its utility in the context of ischemic stroke has not been extensively characterized. We tested the ability of QSM to characterize tissue changes in the transient middle cerebral artery occlusion (tMCAO) model of cerebral ischemia. We acquired high resolution GRE of mice brains at different time points after tMCAO for computation of QSM and MR frequency maps, and compared these maps with DWI and multi-slice multi-echo imaging acquired with the same animals. Prominent vessels with increased magnetic susceptibility were visible on frequency and magnetic susceptibility maps surrounding the lesion at all times (mostly visible at >12h after reperfusion). Immunohistological examination revealed compressed capillaries and prominent vessels after reestablishing reperfusion may indicate a compensatory effect. In addition, on both contrast maps regions of decreased magnetic susceptibility delineated at 24h and 48h after reperfusion that were distinctly different from the lesions seen on maps of the apparent diffusion coefficient (ADC) and T_2 relaxation time constant. Since QSM can be performed without additional acquisition time in the course of acute stroke MRI examination, it may provide complementary information for the diagnostic follow-up of cerebral ischemia.

Introduction

Magnetic resonance imaging (MRI) is an important aid for physicians in the diagnosis and management of patients with acute stroke [1]. The technique offers multiple useful contrasts for assessing hemodynamic function and brain injury. For ischemic stroke, magnetic resonance angiography can identify occlusion of a parent artery [2], and perfusion weighted imaging reveals regional disturbances of cerebral blood supply during hyperacute and acute ischemic stroke [3]. Diffusion weighted imaging (DWI) has been shown to depict the ischemic lesion in the hyperacute, acute and subacute stage after the ischemic insult [4-7]. Assessment of T_1 and T_2 relaxation times has also been used for detecting ischemic damage [8, 9].

Bulk magnetic susceptibility is a fundamental physical property and is a quantitative measure of a materials tendency to interact and with and distort an applied magnetic field. By applying gradient (recalled) echo (GRE) magnetic-resonance based techniques such as T_2*-weighted imaging [10,11], phase imaging [12, 13], and susceptibility weighted imaging (SWI) [14, 15] it became possible to qualitatively assess magnetic susceptibility variations in the brain. For acute stroke MRI, T_2*-weighted imaging and SWI are used for the detection of cerebral microbleeds and hemorrhages [16]. SWI has been used to demonstrate areas of hypoperfusion, and detect acute intravascular embolus [1]. In addition, SWI has been shown to detect asymmetrical veins between ischemic and normal brain tissues, and can give thus information about oxygen metabolism [17-19].

More recently quantitative susceptibility mapping (QSM) has been introduced as post-processing technique for GRE data. QSM uses small magnetic field variations to compute quantitative maps of the corresponding underlying magnetic susceptibility distribution. QSM has been shown to provide complementary anatomical contrast of the brain [20, 21], to help to identify and characterize brain lesions [22, 23], for quantification of tissue iron [24, 25], for assessing functional changes [26], and quantification of contrast agent [27]. For acute stroke QSM has been shown to be able to assess vessel function and oxygen metabolism in patients with acute stroke [18, 28] and an animal model of disease [29].

In the present study, we have tested the ability of QSM and MR frequency mapping to assess tissue changes in the mouse brain after transient middle cerebral artery occlusion (tMCAO). We acquired high resolution GRE, DWI and multi-slice multi-echo imaging data of mice brains at different time points after tMCAO. On post-processed QSM and MR frequency maps we quantified magnetic susceptibility and frequency in prominent vessels and tissue changes in the ischemic and contralateral hemisphere side. In addition, we evaluated the visibility of the ischemic lesions on frequency, magnetic susceptibility maps, apparent diffusion coefficient (ADC) and T_2 relaxation times. Histological and immunohistochemical analysis was performed to attribute morphological changes to the observed changes in the imaging data.

Methods

Animals

All procedures conformed to the national guidelines of the Swiss Federal act on animal protection and were approved by the Cantonal Veterinary Office Zurich (Permit Number: 18-2014 and 49-2011). All procedures fulfill the ARRIVE guidelines on reporting animal experiments. Animals were housed in a temperature controlled room in individually ventilated cages, containing up to 5 animals per cage, under a 12 h dark/light cycle. Paper tissue was given as environmental enrichment. Access to pelleted food (3437PXL15, CARGILL) and water were provided *ad libitum*.

Study design and ischemia model

Seventeen male C57Bl6/J mice (Janvier, France), weighing 20-25g, of 8-10 weeks of age were used. Animals were randomly assigned to the operators (www.randomizer.org) by an independent individual not involved in data acquisition and analysis. We performed surgery and evaluation of all readout parameters, while being blinded to the experimental groups. Anaesthesia was initiated by using 3% isoflurane (Abbott, Cham, Switzerland) in a mixture of O_2 (200 ml/min) and air (800 ml/min) and maintained with 1.5-2% isoflurane. Before the surgical procedure, a local analgesic (Lidocaine, 0.5%, 7 mg/kg) was administered subcutaneously. Temperature was controlled during the surgery and kept constant at 36.5±0.5°C with a feedback-heating controlled pad system. The surgical procedure was carried out as described [30, 31]. The middle cerebral artery was occluded for 1 h. After surgery, buprenorphine was administered as subcutneaous injection every 6-8 h on the day of surgery (Temgesic, 0.1 mg/kg b.w) and thereafter supplied via the drinking water (1 mg/kg) for 36 h.

tMCAO animals were assessed with MRI at 2h (n=3), 4h (n=4), 6h (n=3), 12h (n=4), 24h (n=3) and 48h (n=6) after reperfusion, where the majority of animals were measured at two time points. ADC maps of all investigated mice where inspected. Animals were analyzed when a lesion in ADC maps was present.

Magnetic resonance imaging

MRI measurements were acquired on a Bruker PharmaScan 47/16 (Bruker BioSpin GmbH, Ettlingen, Germany) operating at 4.7T and equipped with a cryogenic transmitter-receive RF coil [32]. During MRI mice were spontaneously breathing under isoflurane anesthesia (1.5%). Body temperature was monitored with a rectal temperature probe (MLT415, ADInstruments, Spechbach, Germany) and kept at 36±0.5°C using a warm water circuit integrated into the animal support.

Anatomical reference data acquired in coronal and sagittal orientations served for accurate positioning of the animal`s head. Global 1st order shimming followed by fieldmap-based local shimming was performed on the mouse brain using the automated MAPshim routine to reduce field inhomogeneities.

For DWI, a two-dimensional (2D) multi-segment spin echo sequence with echo planar imaging readout (SE-EPI) was used. The scan parameters were: field-of-view (FOV) = 17 mm×14 mm, acquisition matrix=128x128, nominal in-plane voxel size=133 µm×109 µm, 12 slices of 1 mm thickness and an interslice distance=1.3 mm, number of segments=4, echo time (TE)=27.5 ms, and repetition time (TR)=3000 ms. Diffusion-encoding was applied in x-, y- and z-direction (gradient pulse duration=4ms, gradient pulse separation=14 ms) with b-values of 100, 200, 400, 600, 800, and 1000 s/mm^2, respectively. The acquisition time was 3 min 48s.

To assess the T_2 relaxation time of brain tissue, a 2D Carr-Purcell-Meiboom-Gill multi-slice multi-echo imaging was performed with FOV=20 mm × 20 mm, acquisition matrix=100×100, nominal in-plane voxel size 200 µm×200 µm, 14 echoes with TE_1=12ms and an inter-echo time of 12ms, TR=2783ms, and four averages. The acquisition time was 14 min and 6s.

For phase imaging and QSM a 3D multi-echo GRE sequence was applied using a FOV=25.6 mm×25.6 mm×8 mm and an acquisition matrix=256×256×80, resulting in an effectively isotropic spatial resolution of 100 µm×100 µm×100 µm. Four echoes were recorded (TE_{1-4} = 4.5/10.5/16.5/22.5 ms) with TR=100 ms, flip angle=15°, monopolar echo readout and no averaging. The acquisition time was 25 min 36s.

Data processing

ADC maps were calculated on a pixel-by-pixel basis by linear regression analysis using the model function:

$$\ln(S(b)/S_0) = -b \cdot ADC \qquad (1)$$

where $S(b)$ is the measured signal intensity at a specific b-value (b) and S_0 is the signal intensity in the absence of a diffusion gradient (b=0).

The T_2 relaxation time was computed for each pixel using Paravision software (Bruker) by fitting the spin-echo magnitude signal, S, at each TE, to a mono-exponential decay function:

$$S(TE) = S_0 \cdot \exp\left(-\frac{TE}{T_2}\right), \qquad (2)$$

where both S_0, the signal at TE=0, and T_2, the irreversible transverse relaxation time, are fitted.

Single-channel GRE magnitude images were combined using the sum-of-squares method [33], whereas single-channel GRE phase images were combined by taking the argument of the complex summed single-channel images after subtracting the channel-dependent phase offset estimated in the center of the three-dimensional volume of the first echo [34]. Quantitative susceptibility maps were computed based on these combined phase images. To this end, the combined phase images for each echo were unwrapped using a 3D best-path algorithm [35], divided by $(2\pi \cdot TE)$ to obtain the Larmor frequency variation in Hz, and then combined across the different TEs in an optimized way that takes into account the local echo-time dependent contrast-to-noise ratio of the Larmor frequency images [36]. Background frequency contributions were eliminated using sophisticated harmonic artifact removal for phase data (SHARP)[37], with 10 different spherical kernels with varying radii ranging from 100 µm to 1000 µm [38], employing a regularization parameter for truncated singular value decomposition of 0.05. Susceptibility mapping was performed based on SHARP-processed frequency images using homogeneity enabled incremental dipole inversion (HEIDI) [20].

Volume-of-interest analysis

For quantitative evaluation volumes-of-interest (VOIs) were drawn around three individual vessel structures that appeared prominent on both the ipsilateral side and the contralateral side if visible, and around one lateral ventricle using MRIcron (www.sph.sc.edu/comd/rorden/mricron/). In addition, VOIs were drawn around the suspected lesion, ipsi- and contralateral striatum and cortex.

Determination of

VOIs were drawn around Significant deviations from the signal distribution were identified in the ischemic hemisphere compared to the unaffected, contralateral hemisphere on all contrasts using Paravision (Bruker) and MRIcron. In addition, VOIs were drawn around the remaining ipsilateral hemisphere and the contralateral hemisphere. The extent of the areas of regional contrast change were calculated edema-corrected as described [39].

Immunohistochemistry

Mice were euthanized at 12h (n=2), 24h (n=3) and 48h (n=2) after reperfusion. Animals were deeply anesthetized by intraperitoneal injection of ketamine/xylazine/ acepromazine maleate (100/20/3 mg/kg body weight) and decapitated. Brains were immediately removed and snap-frozen in 2-methylbutane (Sigma-Aldrich, Switzerland) cooled with dry ice to -30°C and stored at -80°C until processing. They were then thawed and fixed in 4% paraformaldehyde (PFA) for 48 h, than trimmed (coronal section) and routinely paraffin wax embedded.

Consecutive sections (3-5 µm) were prepared and, after antigen retrieval via incubation in citrate buffer (pH 6.0) for 20 min at 98°C, incubated, with rabbit anti-mouse collagen IV (Cat # 2150-1470, AbD Serotec, dil 1:200) for 15-18 h at 4°C. Subsequently, they were incubated with the secondary antibodies (anti-goat horseradish peroxidase, Dako, and Envision rabbit, Dako, respectively).

Statistical analysis

Statistical analysis was performed using SigmaPlot 12.5 (Systat Software, San Jose, CA). Frequency values and susceptibility differences of vessels were compared with a Mann-Whitney Rank Sum test while comparisons between different brain regions were made using an analysis of variance, followed by Holm-Sidak *post hoc* test for multiple comparisons. Lesion volumes between different contrasts were compared with Student's t-test.

Results

All post-processed images are made available in a data repository (DOI upon publication).

Prominent vessels within the ischemic hemisphere on frequency and susceptibility maps

One mouse was excluded from the analysis because no ADC lesion was visible. GRE data of the brain of mice that underwent 1h of tMCAO and different periods of reperfusion were inspected. Vessels with high frequency values and magnetic susceptibility were prominent on background-corrected frequency maps and magnetic susceptibility maps of the ischemic hemisphere (Figure 1 and 2, white arrows). On frequency maps these prominent vessels appeared often as white structures surrounded by a dark rim and were mainly found in the ipsilateral hemisphere in the territory supplied by the middle cerebral artery (MCA). On the contralateral hemisphere vessel-like structures were occasionally observed, but were only faintly visible against the tissue background (for example Figure 4, 6h after reperfusion). Moreover, the prominent vessels in the ipsilateral hemisphere appeared larger in diameter than vessels on the contralateral side. In the ischemic hemisphere of mice acquired at 12h, 24h and 48h after reperfusion the number of prominent vessels was increased compared to mice acquired at 2h, 4h and 6h after reperfusion.

VOI analysis revealed significantly higher frequencies at 2h, 4h and 48h after reperfusion and higher difference in magnetic susceptibility (relative to CSF) at 2h and 4h after reperfusion in suspected vessels of the ischemic ipsilateral side compared to the contralateral hemisphere (Figure 3 a, b).

Immunhistological examination demonstrated that larger vessels appeared dilated compared to the contralateral side (Figure 3 c). Upon higher magnification capillaries showed swollen endothelial cells and narrowing of the vessel lumen (Figure 3 d) in comparison to the capillaries in the controalaterial hepmisphere in the same location, where the vascular lumen is obvious (not shown).

Detection of tissue changes on frequency and susceptibility maps

Inspection of the background-corrected frequency maps revealed areas of decreased frequency values in the ipsilateral hemisphere of tMCAO mice at all time points investigated (Figure 1 and 2, dotted line). The contrast was more apparent at 24h and 48h after reperfusion compared to earlier time points. Similarly, in quantitative susceptibility maps areas of low magnetic susceptibility values were observed in tMCAO mice at 24h and 48h after reperfusion, while at earlier time points such areas were only occasionally visible (Figure 1 and 2). Areas of decreased frequency values were found to be confined within the MCA territory; however, the location and extent

largely varied within the groups of animals investigated at an individual time point and between different time points.

Quantitative analysis demonstrated that frequency values were significantly different between the areas of regional tissue changes and the contralateral striatum at all time points, while for differences in magnetic susceptibility a statistically difference was seen at 48h after reperfusion only (Figure 4). Values of the cortex and striatum in the ipsilateral hemisphere (excluding the area of regional tissue change) were not statistically different from the values of the corresponding areas on the contralateral side for both contrasts.

Extent of regional contrast changes for different MRI contrasts

We measured the extent of contrast changes on frequency and quantitative susceptibility maps and compared it to the cerebral lesion volumes obtained on ADC and T_2 maps (Figure 5 and 6). Among all MRI contrasts the ischemic lesion became first visible on ADC maps as areas of decreased ADC at 2h after reperfusion followed by a steady growth of the lesion until 24h after reperfusion (Figure 5 and Figure 6a). On T_2 maps, a lesion with increased T_2 values became earliest discernable at 6h after reperfusion with growth until 24h after reperfusion (Figure 5 and Figure 4b). The final cerebral hemispheric lesion volumes determined on ADC maps at 48h after reperfusion were not significantly different from the volumes obtained from T_2 maps (mean±SD, 47.4±15.2% ADC vs. 48.3±12.8% T_2; p=0.914). In contrast, regions of contrast change as seen on frequency and quantitative susceptibility maps varied considerably in extent and temporal trajectory. Areas of decreased frequency values and magnetic susceptibility were first discernable at 2h after reperfusion (Figure 5 and 6 c, d). Growth of these regions was only minor on frequency and quantitative susceptibility maps until 48h after reperfusion, and the extent were at all time points lower compared to the lesion volumes seen on ADC and T_2 maps. The final extentafter 48h after reperfusion were significantly lower on quantitative susceptibility compared to frequency maps (19.1±12.0% frequency vs. 4.7±2.4% QSM; p=0.003).

Discussion

In the current study, high resolution MR frequency and quantitative susceptibility maps of the mouse brain were generated after 1h of tMCAO and different time points after reperfusion. On both maps we found prominent vessels with increased magnetic susceptibility. In addition, we observed the delineation of a regional contrast which differed in appearance from the one seen on ADC and T_2 relaxation time constant maps.

Increased susceptibility of prominent cerebral vessels

Prominent vessels in the brain of patients with ischemic stroke have been described on SW images and quantitative susceptibility maps [17, 18, 19]. Their occurrence has been attributed to an increase in oxygen extraction fraction and is correlated with misery perfusion on perfusion maps [18]. The increased oxygen extraction leads to a higher concentration of deoxyhemoglobin in veins which increases the shift in magnetic susceptibility [15]. It has been suggested that prominent vessels are demarcating the penumbra that can be salvaged by vessel recanalization, and that SWI can be used to predict infarct growth [17, 19].

In the current study, we showed that prominent vessels are found in the mouse brain after transient ischemia followed by reperfusion. Vessels were better visible, appeared wider and had significantly higher MR frequency values and larger differences in magnetic susceptibility relative to CSF on the ispilateral side then vessels in the contralateral hemisphere (Figure 1, 2 and 3). Prominent vessels were mainly observed in the surroundings of the core of the lesion. Reperfusion injury is associated in part by incomplete reperfusion of the microvasculature (no-reflow phenomenon). Immunohistological examination indeed demonstrated vasodilation of larger vessels in the ischemic lesion/ipsilateral hemisphere in particular at 24h and 48h after reperfusion and swollen capillaries with narrowing of the lumen at the affected side. These findings are in agreement with other studies which describe capillary constriction and impaired capillary reflow as a consequence of pericyte contraction that persists around microvessels despite reperfusion [40, 41]. Thus, the occurrence of prominent vessels around the lesion after restoration of cerebral blood flow might indicate lower tissue oxygen availability due to compressed capillaries in the ischemic tissue that is compensated for by an increase in oxygen extraction. For stroke treatments this means that recanalization must be accompanied by the reversal of pericyte constrictions and capillary compression that occurred during the ischemic period to fully restore tissue function. The role of prominent vessels after reperfusion need to be further investigated.

Detection of tissue changes on frequency and susceptibility maps

We also observed the occurrence of regions of decreased frequency values and smaller susceptibility differences relative to CSF in tMCAO animals, which has so far not been reported for patients with ischemic stroke. The reason for this observation is that we have performed our study at a higher field strength (4.7T) than the clinical studies (usually 1.5T). As magnetic susceptibility is proportional to the applied magnetic field we were more ably to detect differences in magnetic susceptibility. We also used a higher spatial resolution in this study (100 µm) compared to clinical studies (usually > 1 mm) which allows also to detect smaller morphological features. The loss in signal to noise ratio was compensated for by the use of a high field strength magnet and a cryogenic transmitter-receive RF coil [32]. However, also differences in patient selection and brain anatomy might have played a role.

The appearance of regions of decreased frequency values and smaller susceptibility differences was more apparent at 24h and 48h after reperfusion compared to earlier time points, but was largely variable in individual animals. Moreover, the growth rate and extent of these areas were significantly smaller on frequency and quantitative susceptibility maps compared to the contrast changes seen on ADC and T_2 maps. The underpinnings of these tissue changes detected on susceptibility and frequency maps are currently unclear. Cerebral ischemia is followed by microstructural changes at different stages with edema formation, cell death and tissue destruction and phagocytosis of debris resulting in cavitation with surrounding gliosis [42-44]. However, compartmental water shifts due to cytotoxic and vasogenic edema can be detected by DWI and T_2 mapping, respectively [6,7]. We did not see a spatial congruence between regions of increased T_2 and reduced ADC values with areas of reduced MR frequency values and differences in magnetic susceptibility. Thus both contrasts do likely not represent the ischemic lesion in as distinct to T_2-weighted imaging and ADC, where a good correlation to the histopathological lesion has been demonstrated [45]. It might be speculated that in the regions of decreased frequency and magnetic susceptibility, that are in the center of the suspected lesion, do not extract oxygen [46]. This would lead to an increase in oxygenated blood in that area and thus a diamagnetic shift [47]. However, the relevance of these areas and its cellular underpinnings need to be investigated in further studies.

Taken together, our study revealed characteristic changes in magnetic susceptibility in the mouse brain after transient ischemia followed by reperfusion. The data for QSM can be acquired without additional acquisition time, for example in the course of GRE magnitude or SWI. However, the clinical application of QSM is currently hampered by the numerical complexity and computational cost associated with the post-processing procedure. Novel algorithms have been proposed which allow rapid online reconstruction of susceptibility maps directly after data acquisition, enabling instant evaluation by medical personal [48]. Thus, QSM might be a useful post-processing tool to evaluate GRE data for the diagnosis and during the follow up of patients with ischemic stroke.

Compliance with ethical standards

Funding: This study was by the Swiss National Science Foundation (Grant PZ00P3_136822) and the Hartmann-Müller Foundation.

Conflict of interest: All authors declare that they have no conflict of interest.

Ethical approval: All applicable international and national guidelines for the care and use of animals were followed.

References

1. Kloska SP, Wintermark M, Engelhorn T, Fiebach JB. Acute stroke magnetic resonance imaging: current status and future perspective. Neuroradiology. 2010;52:189-201.
2. Hilger T, Niessen F, Diedenhofen M, Hossmann KA, Hoehn M. Magnetic resonance angiography of thromboembolic stroke in rats: indicator of recanalization probability and tissue survival after recombinant tissue plasminogen activator treatment. J Cereb Blood Flow Metab 2002;22:652-62.
3. Kucharczyk J, Mintorovitch J, Asgari HS, Moseley M. Diffusion/perfusion MR imaging of acute cerebral ischemia. Magn Reson Med 1991;19:311-5.
4. Moseley ME, Cohen Y, Mintorovitch J, Chileuitt L, Shimizu H, Kucharczyk J, et al. Early detection of regional cerebral ischemia in cats: comparison of diffusion- and T2-weighted MRI and spectroscopy. Magn Reson Med 1990;14:330-46.
5. Davis, D., J. Ulatowski, S. Eleff, M. Izuta, S. Mori, D. Shungu , et al. Rapid monitoring of changes in water diffusion coefficients during reversible ischemia in cat and rat brain. Magn Reson Med 1994;31:454-60.
6. Kato H, Kogure K, Ohtomo H, Izumiyama M, Tobita M, Matsui S, et al. Characterization of experimental ischemic brain edema utilizing proton nuclear magnetic resonance imaging. J Cereb Blood Flow Metab 1986;6:212-21.
7. Benveniste H, Hedlund LW, Johnson GA. Mechanism of detection of acute cerebral ischemia in rats by diffusion-weighted magnetic resonance microscopy. Stroke 1992;23:746-54.
8. Calamante F, Lythgoe MF, Pell GS, Thomas DL, King MD, Busza AL, et al. Early changes in water diffusion, perfusion, *T*1, and *T*2 during focal cerebral ischemia in the rat studied at 8.5 T. Magn Reson Med 1999;41:479-85.
9. Grohn OHJ, Kettunen MI, Makela HI, Penttonen M, Pitkanen A, Lukkarinen JA, et al. Early detection of irreversible cerebral ischemia in the rat using dispersion of the magnetic resonance imaging relaxation time, T1rho. J Cereb Blood Flow Metab 2000;20:1457-66.
10. Li TQ, van Gelderen P, Merkle H, Talagala L, Koretsky AP, Duyn JH. Extensive heterogeneity in white matter intensity in high-resolution T2*-weighted MRI of the human brain at 7.0 T. Neuroimage 2006;32:1032-40.
11. Pu Y, Liu Y, Hou J, Fox PT, Gao JH. Demonstration of the medullary lamellae of the human red nucleus with high-resolution gradient-echo MR imaging. Am. J. Neuroradiol 2000;21:1243-7.
12. Budde J, Shajan G, Hoffmann J, Uğurbil K, Pohmann R. Human imaging at 9.4 T using T(2)*-, phase-, and susceptibility-weighted contrast. Magn. Reson. Med. 2011;65:544-50.

13. Rauscher A, Sedlacik J, Barth M, Mentzel HJ, Reichenbach JR. Magnetic susceptibility-weighted MR phase imaging of the human brain. Am J Neuroradiol 2005;26:736-42.
14. Haacke EM, Xu Y, Cheng YCN, Reichenbach JR. Susceptibility weighted imaging (SWI). Magn Reson Med 2004;52:612-8.
15. Reichenbach JR, Haacke EM. High resolution BOLD venographic imaging: a window into brain function. NMR Biomed 2001;14:453-67.
16. Bai Q, Zhao Z, Sui H, Xie X, Chen J, Yang J, et al. Susceptibility-weighted imaging for cerebral microbleed detection in super-acute ischemic stroke patients treated with intravenous thrombolysis. Neurol Res 2013;35:586-93.
17. Kao HW, Tsai FY, Hasso AN. Predicting stroke evolution: comparison of susceptibility-weighted MR imaging with MR perfusion. Eur Radiol 2012;22:1397-403.
18. Luo Y, Gong Z, Zhou Y, Chang B, Chai C, Liu T, et al.. Increased susceptibility of asymmetrically prominent cortical veins correlates with misery perfusion in patients with occlusion of the middle cerebral artery. Eur Radiol. 2017,27:2381-90.
19. Chen CY, Chen CI, Tsai FY, Tsai PH, Chan WP. Prominent vessel sign on susceptibility-weighted imaging in acute stroke: prediction of infarct growth and clinical outcome. PLoS One 2015;10:e0131118.
20. Schweser F, Sommer K, Deistung A, Reichenbach JR. Quantitative susceptibility mapping for investigating subtle susceptibility variations in the human brain. Neuroimage 2012;62:2083-100.
21. Deistung A, Schäfer A, Schweser F, Biedermann U, Turner R, Reichenbach JR. Toward in vivo histology: a comparison of quantitative susceptibility mapping (QSM) with magnitude-, phase-, and R2*-imaging at ultra-high magnetic field strength. Neuroimage 2013;65:299-314.
22. Schweser F, Deistung A, Lehr BW, Reichenbach JR. Differentiation between diamagnetic and paramagnetic cerebral lesions based on magnetic susceptibility mapping. Med Phys 2010;37:5165-78.
23. Klohs J, Deistung A, Schweser F, Grandjean J, Dominietto M, Waschkies C, et al. Detection of cerebral microbleeds with quantitative susceptibility mapping in the ArcAbeta mouse model of cerebral amyloidosis. J Cereb Blood Flow Metab 2011;31:2282-92.
24. Langkammer C, Schweser F, Krebs N, Deistung A, Goessler W, Scheurer E, et al. Quantitative susceptibility mapping (QSM) as a means to measure brain iron? A post mortem validation study. Neuroimage 2012;62:1593-1599.
25. van Bergen JM, Li X, Hua J, Schreiner SJ, Steininger SC, Quevenco FC, et al.. Colocalization of cerebral iron with Amyloid beta in Mild Cognitive Impairment. Sci Rep 2016;6:35514.

26. Fan AP, Schäfer A, Huber L, Lampe L, von Smuda S, Möller HE, et al. Baseline oxygenation in the brain: Correlation between respiratory-calibration and susceptibility methods. Neuroimage 2016;125:920-931.
27. Klohs J, Deistung A, Ielacqua GD, Seuwen A, Kindler D, Schweser F, et al. Quantitative assessment of microvasculopathy in arcAβ mice with USPIO-enhanced gradient echo MRI. J Cereb Blood Flow Metab. 2016;36:1614-24.
28. Uwano I, Kudo K, Sato R, Ogasawara K, Kameda H, Nomura JI, et al. Noninvasive assessment of oxygen extraction fraction in chronic ischemia using quantitative susceptibility mapping at 7 Tesla. Stroke 2017;48:2136-2141.
29. Hsieh MC, Tsai CY, Liao MC, Yang JL, Su CH, Chen JH. Quantitative susceptibility mapping-based microscopy of magnetic resonance venography (QSM-mMRV) for in vivo morphologically and functionally assessing cerebromicrovasculature in rat stroke model. PLoS One 2016;11:e0149602.
30. Vaas M, Enzmann G, Perinat T, Siler U, Reichenbach J, Licha K, et al.. Non-invasive near-infrared fluorescence imaging of the neutrophil response in a mouse model of transient cerebral ischaemia. J Cereb Blood Flow Metab. 2017;37:2833-47.
31. Vaas M, Ni R, Rudin M, Kipar A, Klohs J. Extracerebral tissue damage in the intraluminal filament mouse model of middle cerebral artery occlusion. Front Neurol.2017;8:85.
32. Ratering D, Baltes C, Nordmeyer-Massner J, Marek D, Rudin M. Performance of a 200-MHz cryogenic RF probe designed for MRI and MRS of the murine brain. Magn Reson Med 2008;59:1440-47.
33. Roemer PB, Edelstein WA, Hayes CE, Souza SP, Mueller OM. The NMR phased array. Magn Reson Med 1990;16:192-225.
34. Hammond KE, Lupo JM, Xu D, Metcalf M, Kelley DA, Pelletier D, et al. Development of a robust method for generating 7.0 T multichannel phase images of the brain with application to normal volunteers and patients with neurological diseases. Neuroimage 2008;39:1682-92.
35. Abdul-Rahman HS, Gdeisat MA, Burton DR, Lalor MJ, Lilley F, Moore CJ. Fast and robust three-dimensional best path phase unwrapping algorithm. Appl Opt 2007;46:6623-35.
36. Wu B, Li W, Avram AV, Gho SM, Liu C. Fast and tissue-optimized mapping of magnetic susceptibility and T2* with multi-echo and multi-shot spirals. NeuroImage 2012;59:297-305.
37. Schweser F, Deistung A, Lehr BW, Reichenbach JR. Quantitative imaging of intrinsic magnetic tissue properties using MRI signal phase: an approach to in vivo brain iron metabolism? Neuroimage 2011;54:2789-807.

38. Li W, Wu B, Liu C. Quantitative susceptibility mapping of human brain reflects spatial variation in tissue composition. Neuroimage 2011;55:1645-56.

39. Gerriets T, Stolz E, Walberer M, Müller C, Kluge A, Bachmann A, et al.. Noninvasive quantification of brain edema and the space-occupying effect in rat stroke models using magnetic resonance imaging. Stroke 2004;35:566-71.

40. Yemisci M, Gursoy-Ozdemir Y, Vural A, Can A, Topalkara K, Dalkara T. Pericyte contraction induced by oxidative-nitrative stress impairs capillary reflow despite successful opening of an occluded cerebral artery. Nat Med 2009;15:1031-7.

41. Hall CN, Reynell C, Gesslein B, Hamilton NB, Mishra A, Sutherland BA, et al. Capillary pericytes regulate cerebral blood flow in health and disease. Nature 2014;508:55-60.

42. Garcia JH, Yoshida Y, Chen H, Li Y, Zhang ZG, et al.. Progression from ischemic injury to infarct following middle cerebral artery occlusion in the rat. Am J Pathol. 1993;142:623-35.

43. Ito D, Tanaka K, Suzuki S, Dembo T, Fukuuchi Y. Enhanced expression of Iba1, ionized calcium-binding adaptermolecule 1, after transient focal cerebral ischemia in rat brain. Stroke 2001;32:1208-15.

44. Sun L, Kuroiwa T, Ishibashi S, Miki K, Li S, Xu H, et al. Two region-dependent pathways of eosinophilic neuronal death after transient cerebral ischemia. Neuropathology 2009;29:45-54.

45. Palmer GC, Peeling J, Corbett D, Del Bigio MR, Hudzik TJ. T2-weighted MRI correlates with long-term histopathology, neurology scores, and skilled motor behavior in a rat stroke model. Ann N Y Acad Sci 2001;939:283-96.

46. Heiss WD, Huber M, Fink GR, Herholz K, Pietrzyk U, Wagner R, Wienhard K. Progressive derangement of periinfarct viable tissue in ischemic stroke. J Cereb Blood Flow Metab 1992;12:193-203.

47. Pauling L, Coryell CD. The magnetic properties and structure of hemoglobin, oxyhemoglobin and carbonmonoxyhemoglobin. Proc Natl Acad Sci USA 1936;22:210-16.

48. Schweser F, Deistung A, Sommer K, Reichenbach JR. Toward online reconstruction of quantitative susceptibility maps: superfast dipole inversion. Magn Reson Med. 2013;69:1582-94.

Figure caption

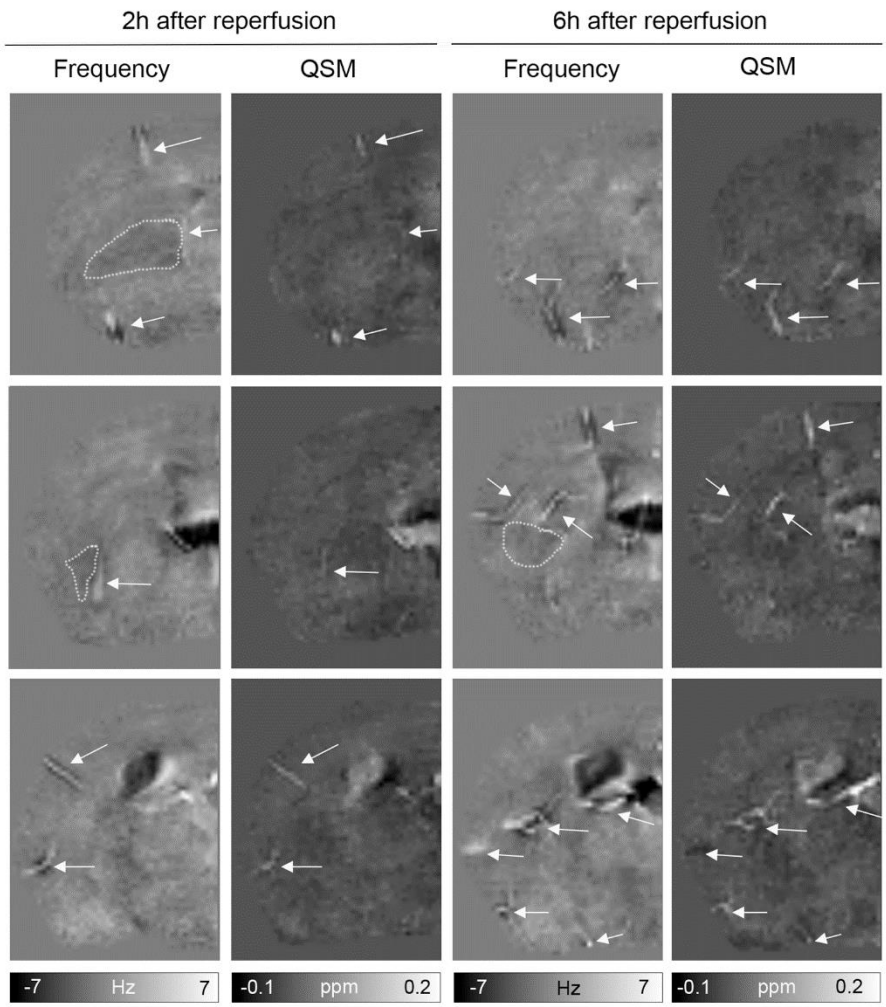

Fig. 1 Few prominent vessels and lesion delineation are apparent on frequency and quantitative susceptibility maps at early time points after reperfusion. Representative axial background-corrected frequency maps and quantitative susceptibility maps (QSM) of the ischemic hemisphere of a mouse subjected to 1h of tMCAO and 2h and 6h of reperfusion are displayed. For both contrasts three cross-sections taken from the ischemic territory (approximately between Bregma 0.14 and -0.82 mm) are shown. Prominent vessels are seen with high MR frequencies and higher magnetic susceptibilities and are presumed to be cerebral blood vessels with high amounts of deoxyhemoglobin (white arrows). Lesions showing decreased frequencies are also discernable (enclosed by white dotted line)

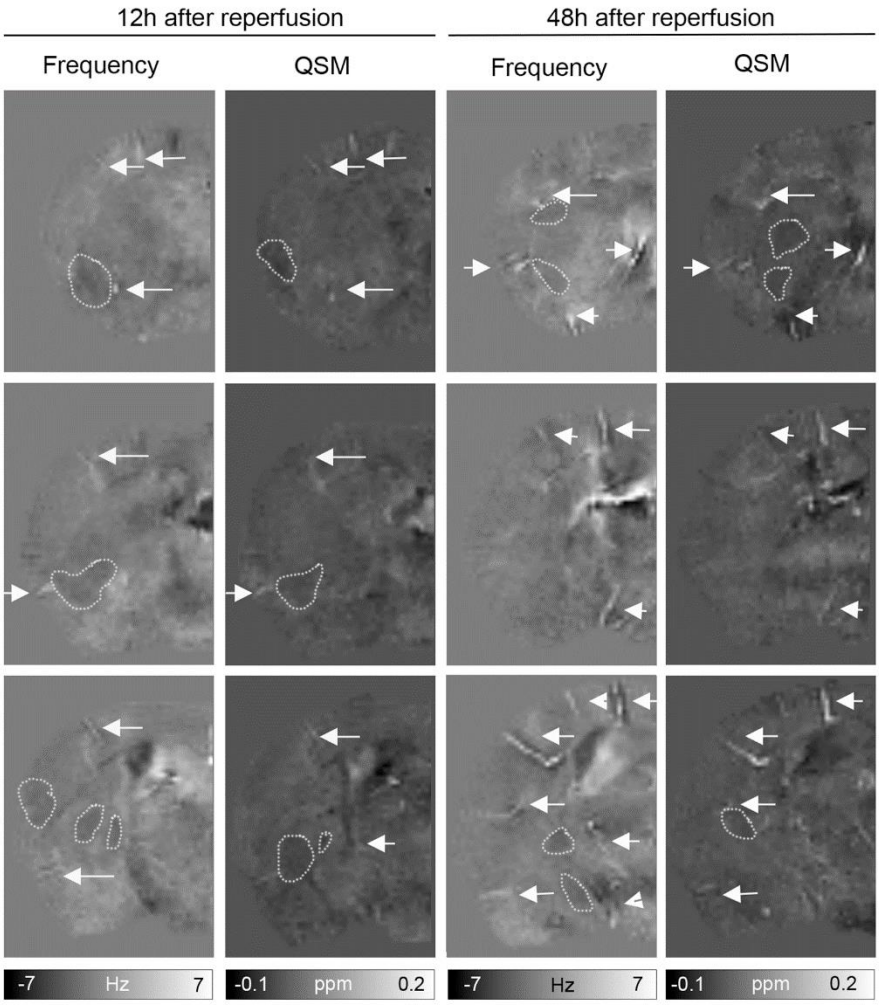

Fig. 2. Increased number of prominent vessels and larger lesions become observable at later time points after reperfusion. Three cross-sections of frequency maps and quantitative susceptibility maps (QSM) of the ischemic hemisphere of a mouse subjected to 1h of tMCAO and 12h and 48h of reperfusion are depicted. Prominent vessels of increased magnetic susceptibility (white arrows) are more frequent compared to earlier time points after reperfusion. Lesions become discernable both on the frequency and susceptibility maps (white dotted line) which increase in extent

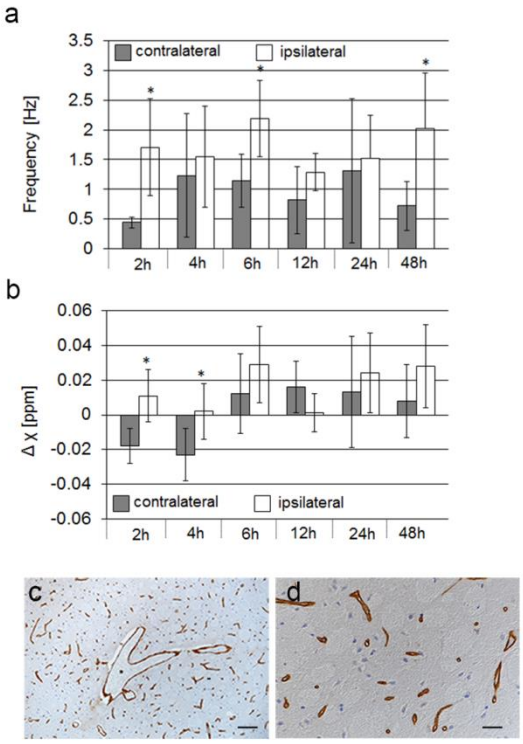

Fig. 3 Quantitative analysis of MRI data and immunohistological assessement of vessels. VOI analysis of **a** MR frequency values and **b** differences in magnetic susceptibility in suspected vessels on the ischemic ipsilateral and contralateral hemisphere at different time points after 1h of tMCAO. Bars graphs represent mean + SD. *P < 0.05 compared to contralateral side. **c, d** Representative anti-collagen IV immunohistochemistry of the brain at 24h after reperfusion. **c** Larger vessels appear dilated (*). Bar = 100 µm. **d** Higher magnification of the lesion shows swelling of endothelial cells and narrowing of the vessel lumen of capillaries. Bar = 20 µm.

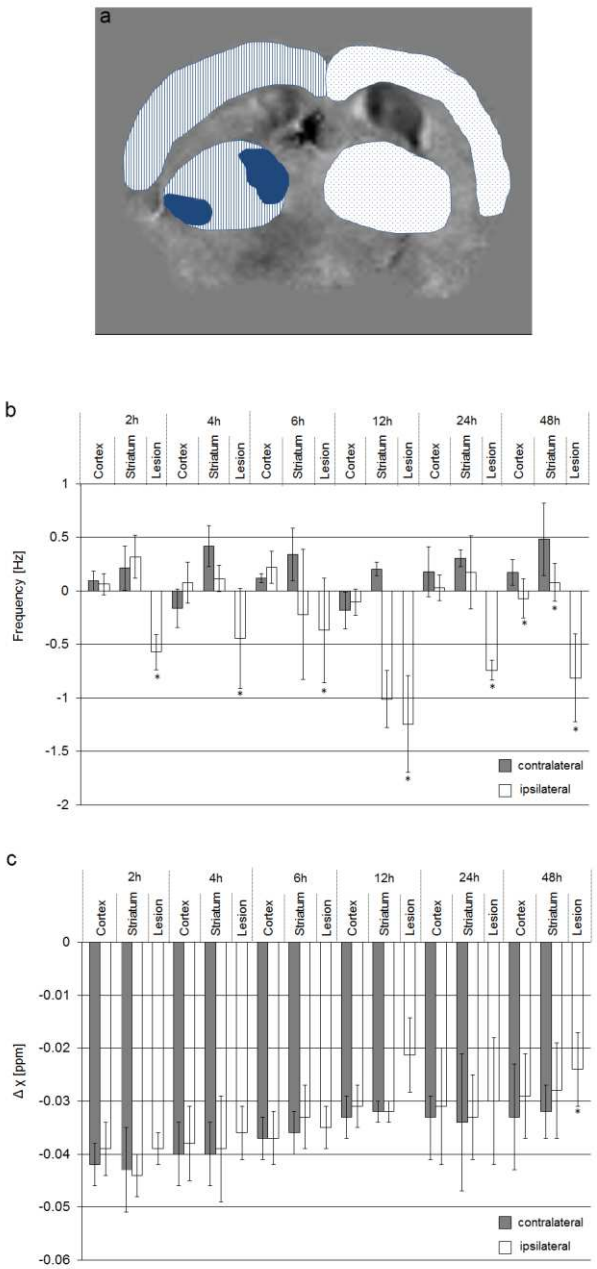

Fig. 4 Quantitative analysis of MRI data of different brain regions. **a** Typical examples of VOI selected on frequency maps. Cortex and striatum where identified on the ischemic hemisphere (*stripped*) and the contralateral (*dotted*) hemisphere excluding areas of markedly reduced frequencies (*blue*). VOI analysis of **b** MR frequency values and **c** differences in magnetic susceptibility in different regions on the ischemic ipsilateral and contralateral hemisphere at different time points after 1h of tMCAO. Bars graphs represent mean + SD. *P < 0.05 compared to contralateral side.

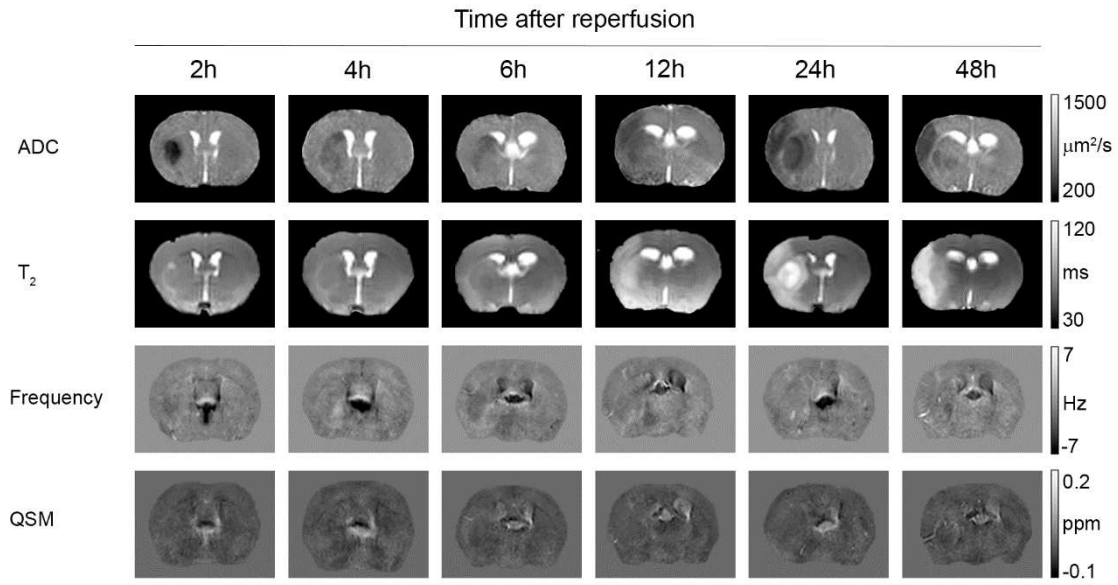

Fig. 5 Contrast changes seen on parametric maps of the ADC, T_2 relaxation time constant, background-corrected MR frequency, and quantitative susceptibility (QSM) following 1h of tMCAO and different intervals of reperfusion. The ischemic lesion becomes first apparent on the ADC map as area of significant reduced ADC at 2h after MCAO, before the lesion is delineated by increased T_2 values on T_2 maps at 6h after MCAO. Regional changes in contrast are discernable on MR frequency and quantitative susceptibility maps from 2h after reperfusion onwards, but are comparatively smaller

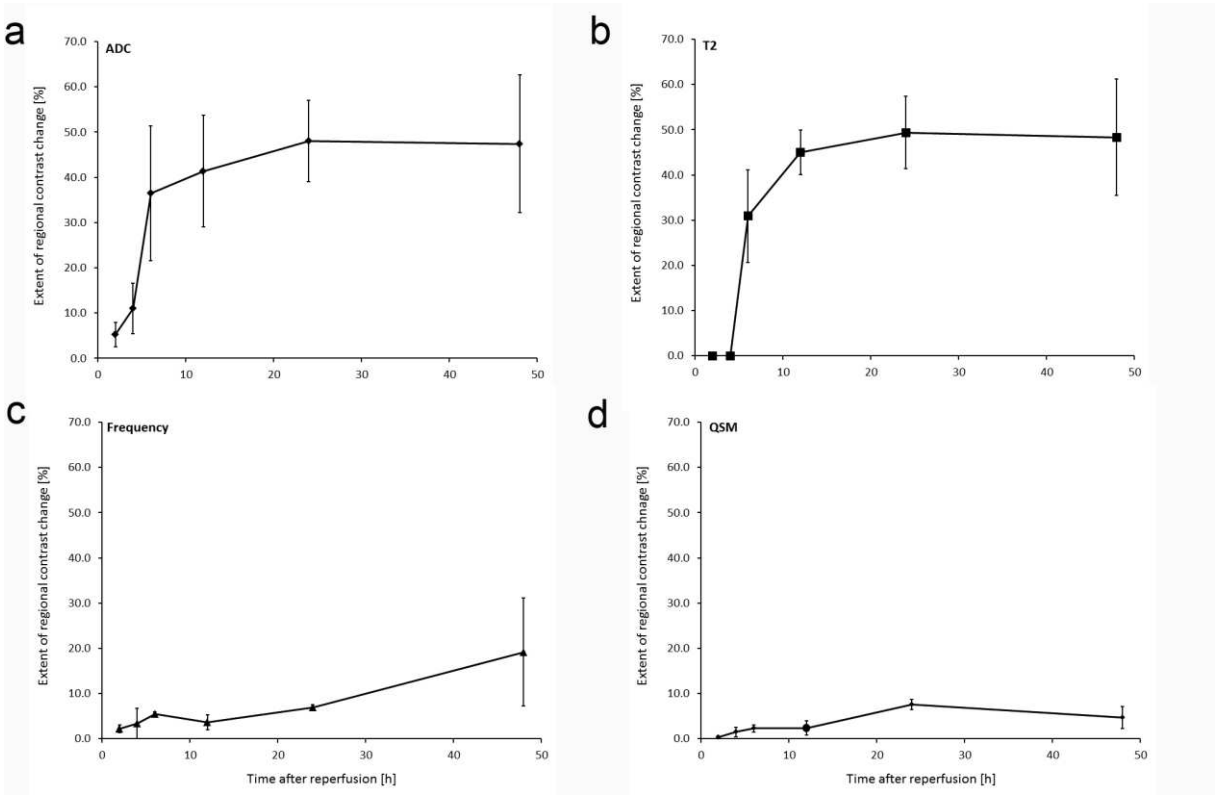

Fig. 6 Temporal evolution of different MRI contrasts after 1h of tMCAO and different periods of reperfusion. Percentage change of the extent of regional contrast change (edema corrected) from a region-of-interest analysis of maps of the ADC (a), T_2 relaxation time constant (b), background-corrected MR frequency (c), and quantitative magnetic susceptibility (d). Displayed are mean values±standard deviations